Methanol–Alkene Reactions in Zeotype Acid Catalysts: Insights from a Descriptor-Based Approach and Microkinetic Modeling

3 AUTHORS:

Rasmus Y Brogaard
University of Oslo
21 PUBLICATIONS **134** CITATIONS

SEE PROFILE

Chuan-Ming Wang
Shanghai Research Institute of Petrochemic…
23 PUBLICATIONS **367** CITATIONS

SEE PROFILE

Felix Studt
Stanford University
92 PUBLICATIONS **2,626** CITATIONS

SEE PROFILE

Methanol−Alkene Reactions in Zeotype Acid Catalysts: Insights from a Descriptor-Based Approach and Microkinetic Modeling

Rasmus Y. Brogaard,[†,∥,§,#] Chuan-Ming Wang,[†,∥,‡,#] and Felix Studt*[,†,∥]

[†]SUNCAT Center for Interface Science and Catalysis, SLAC National Accelerator Laboratory, 2575 Sand Hill Road, Menlo Park, California 94025, United States

[∥]Department of Chemical Engineering, Stanford University, Stanford, California 94305, United States

[‡]Shanghai Research Institute of Petrochemical Technology, SINOPEC, Shanghai 201208, China

[§]inGAP Center for Research Based Innovation, Department of Chemistry, University of Oslo, N-0315 Oslo, Norway

S *Supporting Information*

ABSTRACT: We recently proposed the ammonia heat of adsorption as a reactivity descriptor in solid acid catalysis, using it to predict the activity of zeotype catalysts in the propene−methanol reaction (*J. Phys. Chem. Lett.* **2014**, *5*, 1516−1521). Here we extend the approach to a series of alkene reactants, establishing transition state energy scaling relations for ethene and butenes. Using these relations in connection with microkinetic modeling, we predict a change in reaction pathway as a function of acid-site reactivity and alkene size. The results illustrate the potential of the descriptor-based approach to model acid-catalyzed reactions and efficiently screen for improved solid acid catalysts.

KEYWORDS: *acid catalysis, porous materials, density functional theory, ammonia adsorption, scaling relations, alkene methylation, methanol-to-hydrocarbon conversion*
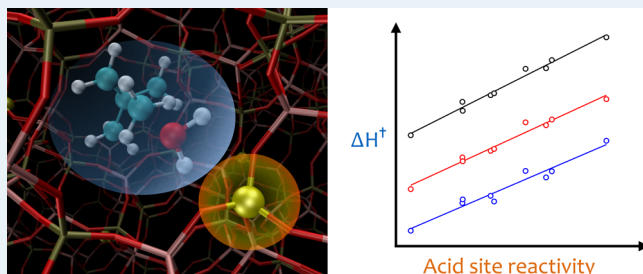
The in silico design of catalysts is one of the ultimate goals in the field of heterogeneous catalysis as such a design has the potential to speed up the discovery of new catalytic materials tremendously.[1] The design strategy is usually based on the identification of key descriptors that determine the catalytic activity and selectivity of materials allowing for fast screening of new leads. The first examples of the in silico discovery of new catalysts have already been reported for (transition-)metal-based materials.[2−5] Structure−activity relationships have also been investigated in porous catalysts with isolated sites.[6−10] Recently, we reported a descriptor-based approach for solid-acid catalysts using the ammonia heat of adsorption, ΔH_{NH3}, as a measure of the reactivity of Brønsted acid sites.[11] The deprotonation energy (DPE) is usually used as a rigorous measure of Brønsted acid *strength*.[10,12−17] As an extension, we proposed ΔH_{NH3} as a quantitative descriptor of the *reactivity* of Brønsted sites in solid acid catalysts, as this measure captures the interactions that determine the stability of molecular transition states and intermediates.[11] Using microkinetic modeling, it was possible to calculate the turnover frequency (TOF) for the propene−methanol reaction in zeotype catalysts as a function of ΔH_{NH3}.[11] Although the previous work focused on that particular reaction, this study aims at extending the approach to several alkene−methanol reactions related to the methanol-to-hydrocarbon (MTH) process.[18−20] The reactions described herein are key reactions of the MTH process, a process that has attracted renewed

interest as it can be seen as a cornerstone in a society where hydrocarbon like olefins and liquid fuels are derived from resources other than oil.[18,21]

As in the previous work, we focus on zeotype materials with the CHA framework topology[22] and alter the reactivity of acid sites by isomorphic substitution of framework atoms (one per unit cell). We adopt a nomenclature where Me-CHA denotes a substituted zeolite. Likewise, a substituted aluminophosphate material is denoted Me-AlPO-34. Hence, Al-CHA and Si-AlPO-34 denote the conventional H-SSZ-13 and H-SAPO-34 materials, respectively. This work focuses on the individual reactions between methanol on the one hand and ethene, propene, isobutene, 1-butene, and 2-butene on the other. These and similar reactions have been extensively investigated both experimentally and theoretically in a wide range of zeolites.[23−30] Generally, two reaction pathways are discussed (see Scheme 1).[31] In the concerted pathway, the alkene reacts with methanol in a single elementary step. In the stepwise pathway, methanol first reacts with the Brønsted acid site to form a surface methyl group, which subsequently reacts with the alkene. Few theoretical works have compared the pathways,[23,32−35] illustrating that the pathway preference depends on reaction conditions as well as framework topology.
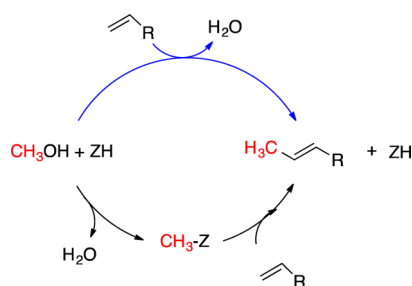
[a]ZH indicates a Brønsted acid site in the zeolite.

The reason is that in general the stepwise pathway is favored in terms of entropy, while the concerted pathway is favored in terms of enthalpy. This means that (1) higher temperatures favor the stepwise pathway, (2) higher pressures favor the concerted pathway, and (3) for a given reaction condition, the zeolite framework determines the enthalpy and entropy contributions and hence also the pathway preference. It follows that without a priori knowledge, theoretical works should in general consider both pathways.

Thus, in this work, we considered the intermediates and transition states of both pathways. We used periodic density functional theory (DFT) calculations employing the BEEF-vdW functional,[36] as this functional has been shown to quantitatively capture the van der Waals (vdW) interactions of alkane adsorption and alkene methylation kinetics in the H-ZSM-22 zeolite.[23,37] The computational setup is identical to the one described previously[11] and briefly outlined in the Methods section. Figure 1 shows the calculated enthalpies of the methylation transition states as a function of ΔH_{NH3} relative to the gas-phase reactants (i.e., methanol and the alkene in question). These enthalpies can be converted to intrinsic (apparent) barriers of the individual reaction steps by instead choosing the alkene−methanol (methanol) adsorption complex as reference state (Tables S1 and S2).

As can be seen, the linear scaling obtained for the propene−methanol reaction[11] can be extended to other alkenes, both linear and branched. In both pathways, the methylation

transition states are stabilized from ethene to propene to isobutene. There are two sources of this stabilization. First, increasing substitution stabilizes the carbocation-like transition state. Second, vdW interactions with the framework stabilize the transition state with increasing alkene size.[23,28,29] With increasing size, alkenes will eventually experience strong repulsive interactions counterbalancing the vdW stabilization and destabilizing the transition state. Our results indicate that the repulsion also increases with alkene substitution; as can be seen in Figure 1A, the transition state involving 2-butene is destabilized slightly compared to that involving 1-butene. Likewise, for isobutene, the transition state is equally stable as for 1-butene, despite isobutene being the most substituted alkene of the two. These two cases illustrate that for a given alkene, there is a subtle interplay between stabilizing and repulsive interactions with the framework. Importantly, however, these interactions are captured by the intercept of the scaling lines and are independent of the acid-site reactivity. Note that the scaling relations show that (the sum of) these interactions are practically identical in the alumino-silicate and -phosphate frameworks; otherwise there would be two scaling relations per species, one for each type of framework. This might not be the case for all molecular species, though, and the issue deserves further investigation.

Turning to the slope of the scaling lines, it is interesting to note that in the concerted pathway it is virtually the same for all alkenes. This leads to the intriguing conclusion that in the concerted pathway all alkenes are equally sensitive to the acid-site reactivity, despite the intrinsic reaction barriers being significantly different. The slope of the scaling lines for the second step in the stepwise pathway is lower and decreases with increasing substitution of the alkene, albeit only slightly. This indicates the following: (1) the transition state in the concerted pathway closely resembles an ion pair like the adsorbed ammonium ion, whereas the transition state of the stepwise pathway does less so; and (2) the resemblance of the latter decreases with increasing substitution of the alkene. Hypothesis (1) is supported by calculated Bader charges in Si-AlPO-34 (Table 1); the degree of charge separation in the transition states for concerted methylation is significantly larger than in the transition states in the stepwise pathway. There is a trend in the Bader charges for the transition states for stepwise methylation, indicating less charge separation with increasing
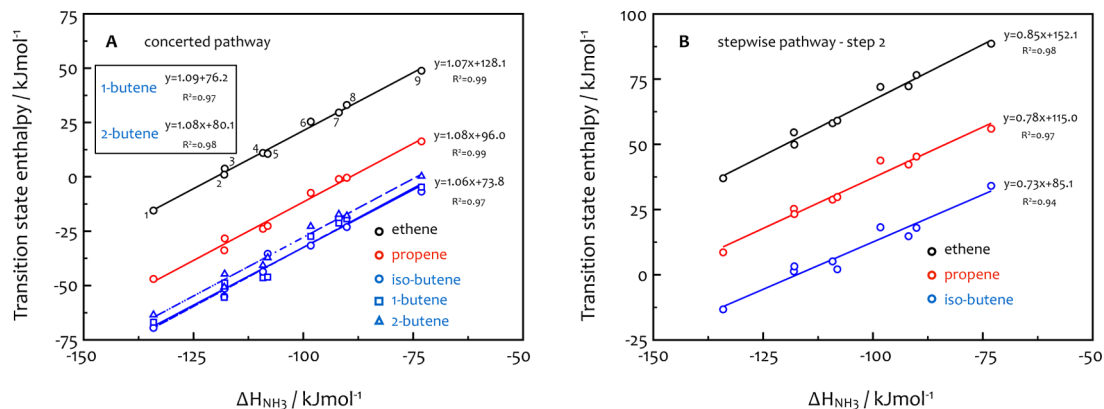

Figure 1. Linear scaling relations between the calculated transition-state enthalpies (referenced to the gas-phase reactants) and calculated ΔH_{NH3} for (A) the concerted and (B) stepwise reaction pathways between methanol and ethene (black circles), propene (red circles), isobutene (blue circles), 1-butene (blue squares), and 2-butene (blue triangles). Materials are (1) Mg-AlPO-34, (2) Zn-AlPO-34, (3) Al-CHA, (4) Ga-CHA, (5) In-CHA, (6) Si-AlPO-34, (7) Sn-AlPO-34, (8) Ge-AlPO-34, (9) Ti-AlPO-34.

Table 1. Bader Charge Analysis Showing the Sum of Excess Charges for the Atoms in the Framework, for Different Molecular Species in Si-AlPO-34[a]

	adsorbates		
	Z-H	Z-CH₃	Z-NH₄
sum of framework charges	−0.59	−0.59	−0.87
	transition states of concerted methylation		
	ethene	propene	isobutene
sum of framework charges	−0.91	−0.89	−0.89
	transition states of stepwise methylation		
	ethene	propene	isobutene
sum of framework charges	−0.78	−0.76	−0.73

[a]The charge of the species hence has the same value with the opposite sign. Z-H: Brønsted acid site, Z-CH₃: surface methyl group, Z-NH₄: adsorbed ammonium ion.

alkene substitution, but the differences are too small to conclusively support hypothesis (2).

Given the insight obtained above, we propose a way to estimate the transition state energies of a larger alkene from that of a smaller one with the same substitution of the double bond. The approach originates from the finding that vdW interactions scale linearly with the number of carbon atoms for adsorption of alkanes in zeolites, with a slope that depends on the framework.[37−42] By extension, this relation applies to the alkyl chains of the alkenes considered in the present work. Consider as an example how the energy of the transition state in the concerted methanol−alkene reaction pathway involving 2-methyl-1-butene can be estimated from that involving isobutene. In the CHA framework, we have determined the vdW contribution per carbon atom in alkyl chains to be 14 kJ/mol (Figure S1). For isobutene, we calculated the energy of the methylation transition state in the stepwise pathway to −32 kJ/mol in Si-AlPO-34. Adding a stabilization of 14 kJ/mol for the extra carbon in the alkyl chain, we arrive at an estimate of −46 kJ/mol for the energy of the corresponding transition state for 2-methyl-1-butene. This compares well to the calculated value of −47 kJ/mol. On the basis of this agreement, we have estimated the energy of the transition state involving 2-methyl-1-butene in the stepwise pathway in Si-AlPO-34 analogously (4 kJ/mol). The CHA framework restricts alkenes larger than 2-methyl-1-butene (repulsive interactions start to dominate), preventing us from investigating the trend for longer alkenes. We further propose that for a given alkene it may be possible to determine the intercept of the corresponding scaling line by calculating the transition state energy in a single material, assuming that the slope of the line is common to all alkenes. In the case of alkene−methanol reactions in the CHA framework, this works for the concerted pathway and to a lesser extent for the stepwise mechanism.

Because the enthalpy and entropy corrections are largely independent of the active site and framework composition for the species involved in this type of reaction (ref 11 and Section S4), the scaling relations established in Figure 1 can be used to estimate free energy profiles. The vibrational frequencies used to derive the thermal corrections do, however, depend highly on the alkene. Unfortunately, it is very cumbersome to calculate vibrational frequencies in periodic DFT calculations, making it intractable for large numbers of intermediates. It is hence desirable to find a way to approximate the thermal corrections for a given alkene, for the descriptor-based approach to be feasible when modeling processes involving numerous alkenes.

This task is outside the scope of the current work and hence left for future research.

The scaling relations were used to calculate TOFs of the alkene methylation reactions in zeotype catalysts. For that purpose, we employed a microkinetic model of individual reactions between methanol and ethene, propene, and isobutene, respectively. The model is constructed analogously to the one developed earlier for the methanol−propene reaction,[11] taking as input the reaction free energy profiles and partial pressures of the gas phase reactants (see Methods section). The model considers both the stepwise and concerted pathways of the methanol−alkene reactions. It was shown for propene that the coverages of alkoxide, alkylium, and reactant/product alkene were negligible,[11] and we therefore only included hydrogen-bonded methanol and chemisorbed methyl groups as intermediates in the present model. Figure 2A
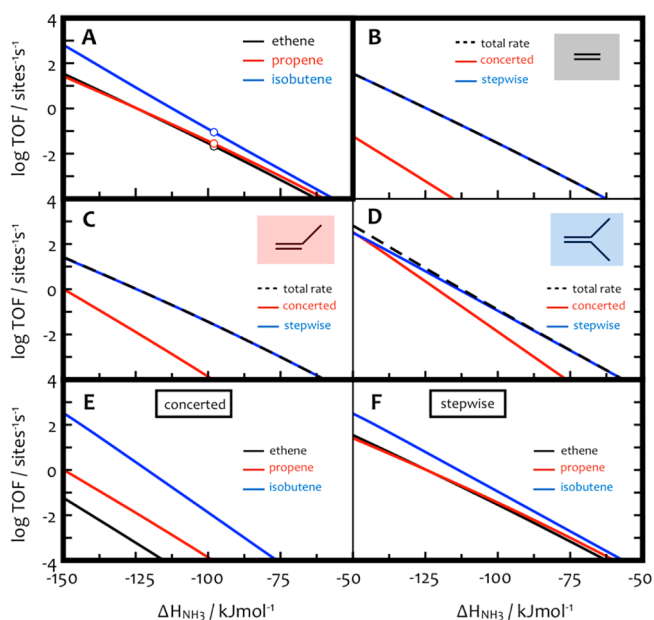

Figure 2. Simulated turnover frequency (TOF, reaction conditions are given in the Methods section) for the methanol−alkene reactions as a function of ΔH_{NH3} for the Me-CHA and Me-AlPO-34 materials. (A) Total rate of the reaction of methanol with ethene (black line), propene (red line) and isobutene (blue line). The calculated value of ΔH_{NH3} for Si-AlPO-34 of −98 kJ/mol is highlighted. (B−D) Rate of the concerted (red lines) and stepwise (blue lines) mechanism along with the total rate (concerted + stepwise mechanism, dashed black lines) for ethene (B), propene (C), and isobutene (D) methylation. (E−F) Comparison of the rates for the concerted (E) and stepwise (F) mechanism for the reaction of methanol with ethene (black lines), propene (red lines), and isobutene (blue lines).

compares the calculated TOFs of the different reactions as a function of the ammonia heat of adsorption. We note that for each alkene the model predicts an optimal acid-site reactivity, above which the TOF starts to decrease (not shown in Figure 2A). However, such high acid-site reactivities are probably not accessible in zeotype materials of the type investigated here, as already pointed out for propene.[11] Individual contributions from the concerted and stepwise mechanism to the total rate are also shown (Figure 2B−F, see also Table 2). While one should be careful with quantitative interpretation of TOFs, we note that trends in theoretically derived TOFs from one material to another are usually well described.[43] The model

predicts Al-CHA (ΔH_{NH3} = −118 kJ/mol) to be more active in alkene−methanol reactions than Si-AlPO-34 (ΔH_{NH3} = −98 kJ/mol), mirroring the relative activities of the catalysts observed in methanol-to-olefin conversion.[44]

In the conventional zeotype Si-AlPO-34 (ΔH_{NH3} = −98 kJ/mol), the stepwise pathway prevails for all alkenes investigated here (see Figure 2 and Table 2), similarly to what was predicted

Table 2. Contributions of the Concerted and Stepwise Pathways to the Total Rate of Methanol−Alkene Reactions in Si-AlPO-34, As Extracted from the Microkinetic Models

	ethene	propene	isobutene
rate stepwise (site^{-1} s^{-1})	2.15×10^{-2}	2.72×10^{-2}	7.99×10^{-2}
rate concerted (site^{-1} s^{-1})	3.91×10^{-6}	9.29×10^{-5}	8.67×10^{-3}
total rate (site^{-1} s^{-1})	2.2×10^{-2}	2.7×10^{-2}	8.9×10^{-2}
contribution stepwise mechanism	1.00	9.97×10^{-1}	9.02×10^{-1}
contribution concerted mechanism	2.0×10^{-4}	3.40×10^{-3}	9.79×10^{-2}

for H-ZSM-22.[23] Interestingly, the predicted rate of the stepwise pathway increases with alkene substitution from ethene to isobutene for which it is saturated. The saturation can be appreciated by manually lowering the barrier for the methylation step in the stepwise pathway from that for isobutene and rerunning the model (results not shown). The resulting methylation rate does not increase, showing that the first step (i.e., the formation of surface methyl groups) is rate determining. The rate of the concerted pathway, however, increases rapidly with substitution of the alkene (see Table 2 and Figure 2E). Hence, the contribution of the concerted pathway increases with alkene size (see Table 2, Figure 2B−D). As the stepwise pathway is eventually limited by the formation of surface methyl groups, the concerted pathway becomes dominant so that the total rate increases with size for alkenes larger than isobutene. Note, however, that this rate increase is expected to be limited, because the stabilization of the transition state with alkene size is somewhat counterbalanced by the increased entropy loss, also known as the compensation effect.[39,45] Finally, notice how the rate of the concerted pathway is more sensitive to acid-site reactivity than that of the stepwise (Figures 2B−D), just as observed in the slopes of the scaling lines of the corresponding transition states (Figure 1).

Having obtained the rates of the reactions from the microkinetic model, we can also derive apparent activation energies

$$E_{app}(T_a) = T_a^2 * (dTOF/dT)_{T_a} \qquad (1)$$

This activation energy is equal to that obtained from an Arrhenius plot, if the latter is strictly linear, and hence enable the most direct comparison between computed and experimentally observed kinetics. This allows us to derive the apparent activation energy as a function of acid-site reactivity (Figure 3). Note that for isobutene the apparent activation energy turns negative for highly reactive acids, because the enthalpies of the transition states are below those of the gas phase reactants (Figure 1). For ethene and propene, where the stepwise pathway dominates (Figure 2), the transition state enthalpies are above the gas phase reactants (Figure 1) and the activation energies stay positive. In other words, for very reactive catalysts like Mg-AlPO-34 (ΔH_{NH3} = −134 kJ/mol), the rate is predicted to increase with temperature for ethene
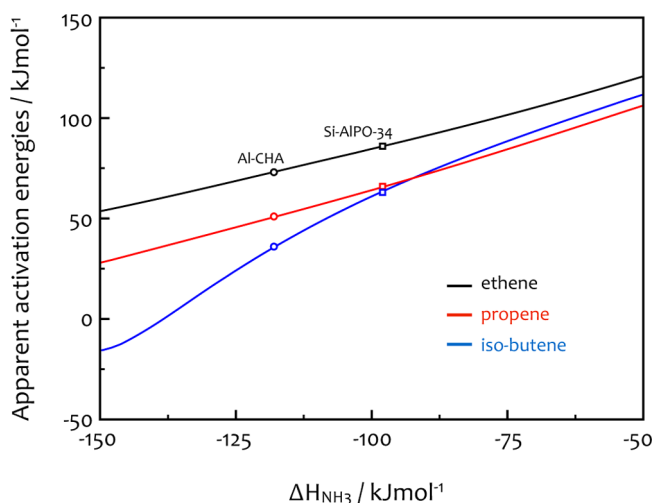

Figure 3. Apparent activation energies for the methylation of ethene (black line), propene (red line), and iso-butene (blue line) as a function of the ammonia heat of adsorption. Apparent activation energies are derived from the microkinetic model (T = 623 K) using eq 1. Values for Al-CHA and Si-AlPO-34 are marked as circles and squares, respectively.

and propene, and decrease for isobutene. No experimental data is available for alkene−methanol reactions in the CHA framework, but Svelle and co-workers have investigated the reactions in zeolite H-ZSM-5.[26,27] The computed activation energies for alkene methylation in the zeolite Al-CHA (Figure 3) express the same trend (ethene = 73 kJ/mol, propene = 51 kJ/mol, and isobutene = 36 kJ/mol) as observed in the experiments (ethene = 103 kJ/mol, propene = 69 kJ/mol, and 1-butene = 45 kJ/mol).

In summary, we have shown a theoretical analysis of the catalytic activity of acidic zeotypes in the alkene−methanol reaction for a series of alkenes. It is clearly shown that ΔH_{NH3} is a remarkably good descriptor of the reactivity of Brønsted acid sites in the zeotypes investigated here, as the energies of all transition states of the alkene methylation reactions scale linearly with ΔH_{NH3}. The intercepts of the scaling lines depend on the size and shape of the alkene, expressing a balance between stabilizing and repulsive interactions. We have shown that the transition state energy of an alkene can be estimated from its chain length and the vdW contribution that is expected from the framework. We furthermore suggest that the transition-state energy of an alkene in a single material can be used to estimate the corresponding energies in multiple materials having the CHA framework simply by calculating ΔH_{NH3}. We have used energy scaling relations in connection with microkinetic modeling to predict a change in preferred reaction pathway (concerted vs stepwise) as a function of acid-site reactivity and reactant alkene, and for larger alkenes we propose a shift in the reaction mechanism from stepwise to concerted.

The work illustrates a simple approach to predict rates of acid-catalyzed reactions, which dramatically reduces the computational effort imposed by DFT calculations by establishing linear energy-scaling relations with ΔH_{NH3} as a descriptor. The approach is particularly useful in microkinetic modeling requiring kinetic parameters for a large amount of elementary steps, which would be intractable to calculate by DFT. We have shown this descriptor-based approach to be applicable to alkene−methanol reactions. So far our analysis is based solely

on methylation of simple alkenes, for which similarity in scaling relations might be anticipated. Due to the high correlation found for these relations, however, we are suggesting that the approach can be extended to other reactions. Further, we propose that a wide range of solid Brønsted acid catalysts express scaling relations using ΔH_{NH3} as a descriptor of the reactivity of Brønsted acid sites. However, ΔH_{NH3} cannot give information about the accessibility of acid sites or shape-selective properties of porous catalysts. Hence, it remains to be seen how the descriptor-based approach can be extended to porous catalysts with multiple different Brønsted acid sites, without having to establish energy-scaling relations for every species at every site. We believe the insight gained from this work clearly justifies further investigations to extend the scope and use of the theoretical framework in research on solid acid catalysis. Finally, we note that catalyst performance is determined not only by the catalytic activity considered here but also by selectivity and catalyst lifetime. Hence, the theoretical framework can provide leads for improved catalysts that supplemented by experimental tests can streamline the process of catalyst discovery.

METHODS

Density functional theory calculations were performed as described in detail previously.[11] Briefly, the calculations were performed with the GPAW package, a real-space grid implementation of the projector augmented-wave method,[46] interfaced with the ASE package.[47] The calculations employed the Bayesian error estimation functional with van der Waals correlation (BEEF-vdW).[36] Bader charge analysis was performed using the algorithm of Henkelman et al.[48] on the all-electron density, as reconstructed from the pseudodensity using GPAW. The CHA and AlPO-34 frameworks were represented by periodic 36T hexagonal cells. Lattice constants were optimized to $a = b = 13.90$ Å, $c = 15.11$ Å for AlPO-34 and $a = b = 13.80$ Å, $c = 14.84$ Å for CHA. Substitution of Si (CHA), P, or Al (AlPO-34) with a metal atom generated one Brønsted acid site per unit cell. Experimentally it is found that the proton is about equally distributed between the O(2) and O(4) sites in Si-AlPO-34.[49] Theoretical studies indicate, however, that the energy differences between the four distinct protonation sites are small (<10 kJ/mol).[50] Here, the hydrogen atom was chosen to be located at the O(2) site in all materials, similar to other theoretical studies on Si-AlPO-34.[51] Unless otherwise indicated, the materials considered were Si-, Ge-, Sn-, Ti-, Mg-, and Zn-AlPO-34 as well as Al-, Ga-, and In-CHA.

Conventional statistical mechanics was used to derive enthalpy and entropy using the thermochemistry module of the ASE package, treating isolated molecules in the rigid rotor harmonic oscillator approximation and employing the harmonic approximation for adsorbates and transition states.[52] As in previous work,[11] the harmonic frequency calculations employed a partial Hessian approach, including the atoms of the molecular species, as well as the H atom of the Brønsted acid site. The harmonic frequencies were obtained for each molecular species in Si-AlPO-34, except for protonated methanol and the transition state for concerted ethene methylation, employing Mg-AlPO-34 and Sn-AlPO-34, respectively (see Explanation Section S1). The single set of frequencies for each species was reused for all other catalysts, assuming the correction from electronic energy to enthalpy and free energy to be independent of framework composition. We validated this assumption for physisorbed 2-butene and

chemisorbed ammonia in recent work[11] and two transition states in this work (see Table S4), finding deviations in entropy contributions to free energies at 623 K to be 7 kJ/mol or less.

The harmonic approximation inherently breaks down for large-amplitude nuclear motions and numerical noise becomes significant, as expressed by the presence of spurious imaginary values among the low frequencies. This occurred for some of the transition states considered in this work, each having one imaginary frequency in addition to the one corresponding to the reaction coordinate. The spurious frequencies were less than 100i cm^{-1} in magnitude (see Table S3). After carefully checking that the associated nuclear motions corresponded largely to translations or rotations of the species, the frequencies were replaced by 12 cm^{-1}. This value is chosen because the entropy contribution from a 12 cm^{-1} harmonic vibration approximates that from a pseudotranslational/rotational degree of freedom, as discussed in detail in previous work on zeolite-catalyzed alkene–methanol reactions.[23] Recent work has shown an alternative approach, improving numerical accuracy by adopting normal-mode coordinates for structure optimization and numerical frequency calculations.[53,54] Calculated enthalpies are stated at 0 K herein, as previous work found for two test cases that the correction from heat capacity is within 6 kJ/mol for temperatures up to 623 K.[11]

The free energy profiles were used as input to the microkinetic model, which was solved using CatMAP,[55] employing the mean-field approximation and a steady-state solution of the rate equations. The model used a temperature of 623 K and partial pressures of methanol, reactant alkene, water, and product alkene of 0.6, 0.2, 0.1, and 0.1 bar, respectively. Apparent activation energies were computed according to eq 1 using forward differences as numerical differentiation scheme. Further details can be found in the Supporting Information.

ASSOCIATED CONTENT

S **Supporting Information**
The following file is available free of charge on the ACS Publications website at DOI: 10.1021/cs5014267.

> Additional computational details; intrinsic and apparent barriers of individual reaction steps; details about the adsorption of alkanes in the CHA framework; assessment of the calculated thermochemical data; illustrations of optimized structures in Si-AlPO-34; technical details and input for the microkinetic modeling (PDF)

AUTHOR INFORMATION

Corresponding Author
*E-mail: studt@slac.stanford.edu.
Author Contributions
#R.Y.B. and C.-M.W. contributed equally to this work.
Notes
The authors declare no competing financial interest.

ACKNOWLEDGMENTS

■ REFERENCES

(1) Nørskov, J. K.; Abild-Pedersen, F.; Studt, F.; Bligaard, T. *Proc. Natl. Acad. Sci. U.S.A.* **2011**, *108*, 937−943.

(2) Greeley, J.; Jaramillo, T. F.; Bonde, J.; Chorkendorff, I.; Nørskov, J. K. *Nat. Mater.* **2006**, *5*, 909−913.

(3) Studt, F.; Abild-Pedersen, F.; Bligaard, T.; Sørensen, R. Z.; Christensen, C. H.; Nørskov, J. K. *Science* **2008**, *320*, 1320−1322.

(4) Alayoglu, S.; Nilekar, A. U.; Mavrikakis, M.; Eichhorn, B. *Nat. Mater.* **2008**, *7*, 333−338.

(5) Studt, F.; Sharafutdinov, I.; Abild-Pedersen, F.; Elkjær, C. F.; Hummelshøj, J. S.; Dahl, S.; Chorkendorff, I.; Nørskov, J. K. *Nat. Chem.* **2014**, *6*, 320−324.

(6) Borges, P.; Pinto, R. R.; Lemos, M. A. N. D. A.; Védrine, J. C.; Derouane, E. G.; Ribeiro, F. R. *J. Mol. Catal. A: Chem.* **2005**, *229*, 127−135.

(7) Pidko, E. A.; van Santen, R. A. *J. Phys. Chem. C* **2009**, *113*, 4246−4249.

(8) Katada, N.; Suzuki, K.; Noda, T.; Sastre, G.; Niwa, M. *J. Phys. Chem. C* **2009**, *113*, 19208−19217.

(9) Niwa, M.; Suzuki, K.; Morishita, N.; Sastre, G.; Okumura, K.; Katada, N. *Catal. Sci. Technol.* **2013**, *3*, 1919−1927.

(10) Macht, J.; Carr, R. T.; Iglesia, E. *J. Catal.* **2009**, *264*, 54−66.

(11) Wang, C.-M.; Brogaard, R. Y.; Weckhuysen, B. M.; Nørskov, J. K.; Studt, F. *J. Phys. Chem. Lett.* **2014**, *5*, 1516−1521.

(12) Brändle, M.; Sauer, J. *J. Am. Chem. Soc.* **1998**, *120*, 1556−1570.

(13) Kramer, G. J.; van Santen, R. A.; Emeis, C. A.; Nowak, A. K. *Nature* **1993**, *363*, 529−531.

(14) van Santen, R. A.; Kramer, G. J. *Chem. Rev.* **1995**, *95*, 637−660.

(15) Macht, J.; Carr, R. T.; Iglesia, E. *J. Am. Chem. Soc.* **2009**, *131*, 6554−6565.

(16) Chu, Y.; Han, B.; Fang, H.; Zheng, A.; Deng, F. *Microporous Mesoporous Mater.* **2012**, *151*, 241−249.

(17) Jones, A. J.; Carr, R. T.; Zones, S. I.; Iglesia, E. *J. Catal.* **2014**, *312*, 58−68.

(18) Olsbye, U.; Svelle, S.; Bjørgen, M.; Beato, P.; Janssens, T. V. W.; Joensen, F.; Bordiga, S.; Lillerud, K. P. *Angew. Chem., Int. Ed.* **2012**, *51*, 5810−5831.

(19) Hemelsoet, K.; Van der Mynsbrugge, J.; De Wispelaere, K.; Waroquier, M.; Van Speybroeck, V. *ChemPhysChem* **2013**, *14*, 1526−1545.

(20) Wang, C.-M.; Wang, Y.-D.; Xie, Z.-K. *J. Catal.* **2013**, *301*, 8−19.

(21) Olah, G. A. *Angew. Chem., Int. Ed.* **2013**, *52*, 104−107.

(22) Baerlocher, C.; McCusker, L. B. *Database of Zeolite Structures*: http://www.izastructure.org/databases/.

(23) Brogaard, R. Y.; Henry, R.; Schuurman, Y.; Medford, A. J.; Moses, P. G.; Beato, P.; Svelle, S.; Nørskov, J. K.; Olsbye, U. *J. Catal.* **2014**, *314*, 159−169.

(24) Mazar, M. N.; Al-Hashimi, S.; Bhan, A.; Cococcioni, M. *J. Phys. Chem. C* **2012**, *116*, 19385−19395.

(25) Hill, I. M.; Ng, Y. S.; Bhan, A. *ACS Catal.* **2012**, *2*, 1742−1748.

(26) Svelle, S.; Rønning, P. O.; Kolboe, S. *J. Catal.* **2004**, *224*, 115−123.

(27) Svelle, S.; Rønning, P. O.; Olsbye, U.; Kolboe, S. *J. Catal.* **2005**, *234*, 385−400.

(28) Svelle, S.; Tuma, C.; Rozanska, X.; Kerber, T.; Sauer, J. *J. Am. Chem. Soc.* **2009**, *131*, 816−825.

(29) Van Speybroeck, V.; Van der Mynsbrugge, J.; Vandichel, M.; Hemelsoet, K.; Lesthaeghe, D.; Ghysels, A.; Marin, G. M.; Waroquier, M. *J. Am. Chem. Soc.* **2011**, *133*, 888−899.

(30) Van der Mynsrugge, J.; De Ridder, J.; Hemelsoet, K.; Waroquier, M.; Van Speybroeck, V. *Chem.—Eur. J.* **2013**, *19*, 11568−11576.

(31) Svelle, S.; Visur, M.; Olsbye, U.; Saepurahman, S.; Bjørgen, M. *Top. Catal.* **2011**, *54*, 897−906.

(32) Vos, A. M.; Nulens, K. H. L.; De Proft, F.; Schoonheydt, R. A.; Geerlings, P. *J. Phys. Chem. B* **2002**, *106*, 2026−2034.

(33) Maihom, T.; Boekfa, B.; Sirijaraensre, J.; Nanok, T.; Probst, M.; Limtrakul, J. *J. Phys. Chem. C* **2009**, *113*, 6654−6662.

(34) Van der Mynsbrugge, J.; Moors, S. L. C.; De Wispelaere, K.; Van Speybroeck, V. *ChemCatChem.* **2014**, *6*, 1906−1918.

(35) Gomes, J.; Head-Gordon, M.; Bell, A. T. *J. Phys. Chem. C* **2014**, *118*, 21409−21419.

(36) Wellendorff, J.; Lundgaard, K. T.; Møgelhøj, A.; Petzold, V.; Landis, D. D.; Nørskov, J. K.; Bligaard, T.; Jacobsen, K. W. *Phys. Rev. B* **2012**, *85*, 235149.

(37) Brogaard, R. Y.; Moses, P. G.; Nørskov, J. K. *Catal. Lett.* **2012**, *142*, 1057−1060.

(38) Göltl, F.; Sautet, P. *J. Chem. Phys.* **2014**, *140*, 154105.

(39) Denayer, J. F.; Baron, G. V.; Martens, J. A.; Jacobs, P. A. *J. Phys. Chem. B* **1998**, *102*, 3077−3081.

(40) Ocakoglu, R. A.; Denayer, J. F. M.; Marin, G. B.; Martens, J. A.; Baron, G. V. *J. Phys. Chem. B* **2003**, *107*, 398−406.

(41) Göltl, F.; Grüneis, A.; Bucko, T.; Hafner, J. *J. Chem. Phys.* **2012**, *137*, 114111.

(42) Eder, F.; Lercher, J. *Zeolites* **1998**, *18*, 75−81.

(43) Medford, A. J.; Wellendorff, J.; Vojvodic, A.; Studt, F.; Abild-Pedersen, F.; Jacobsen, K. W.; Bligaard, T.; Nørskov, J. K. *Science* **2014**, *345*, 197−200.

(44) Svelle, S.; Rønning, P. O.; Olsbye, U.; Kolboe, S. *J. Catal.* **2005**, *234*, 385−400.

(45) Bond, G. C.; Keane, M. A.; Kral, H.; Lercher, J. A. *Catal. Rev. Sci. Eng.* **2000**, *42*, 323−383.

(46) Enkovaara, J.; Rostgaard, C.; Mortensen, J. J.; Chen, J.; Dułak, M.; Ferrighi, L.; Gavnholt, J.; Glinsvad, C.; Haikola, V.; Hansen, H. A.; Kristoffersen, H. H.; Kuisma, M.; Larsen, A. H.; Lehtovaara, L.; Ljungberg, M.; Lopez-Acevedo, O.; Moses, P. G.; Ojanen, J.; Olsen, T.; Petzold, V.; Romero, N. A.; Stausholm-Møller, J.; Strange, M.; Tritsaris, G. A.; Vanin, M.; Walter, M.; Hammer, B.; Häkkinen, H.; Madsen, G. K. H.; Nieminen, R. M.; Nørskov, J. K.; Puska, M.; Rantala, T. T.; Schiøtz, J.; Thygesen, K. S.; Jacobsen, K. W. *J. Phys.: Condens. Matter* **2010**, *22*, 253202.

(47) Bahn, S. R.; Jacobsen, K. W. *Comput. Sci. Eng.* **2002**, *4*, 56−66.

(48) Tang, W.; Sanville, E.; Henkelman, G. *J. Phys.: Condens. Matter* **2009**, *21*, 084204.

(49) Smith, L.; Cheetham, A. K.; Marchese, L.; Thomas, J. M.; Wright, P. A.; Chen, J.; Gianotti, E. *Catal. Lett.* **1996**, *41*, 13−16.

(50) Jeanvoine, Y.; Angyán, J. G.; Kresse, G.; Hafner, J. *J. Phys. Chem. B* **1998**, *102*, 5573−5580.

(51) Hemelsoet, K.; Nollet, A.; Van Speybroeck, V.; Waroquier, M. *Chem.—Eur. J.* **2011**, *17*, 9083−9093.

(52) Cramer, C. J.; *Essentials of Computational Chemistry: Theories and Models*, 2nd ed; Wiley: Chichester, U.K., 2004; Chapter 10.

(53) Piccini, G.; Sauer, J. *J. Chem. Theory Comput.* **2013**, *9*, 5038−5045.

(54) Piccini, G.; Sauer, J. *J. Chem. Theory Comput.* **2014**, *10*, 2479−2487.

(55) Medford, A. J.; Sehested, J.; Rossmeisl, J.; Chorkendorff, I.; Studt, F.; Nørskov, J. K.; Moses, P. G. *J. Catal.* **2014**, *309*, 397−407.